Volume 2 | Number 27 | 21 July 2014 | Pages 10315–10698

Journal of Materials Chemistry A

Materials for energy and sustainability

www.rsc.org/MaterialsA

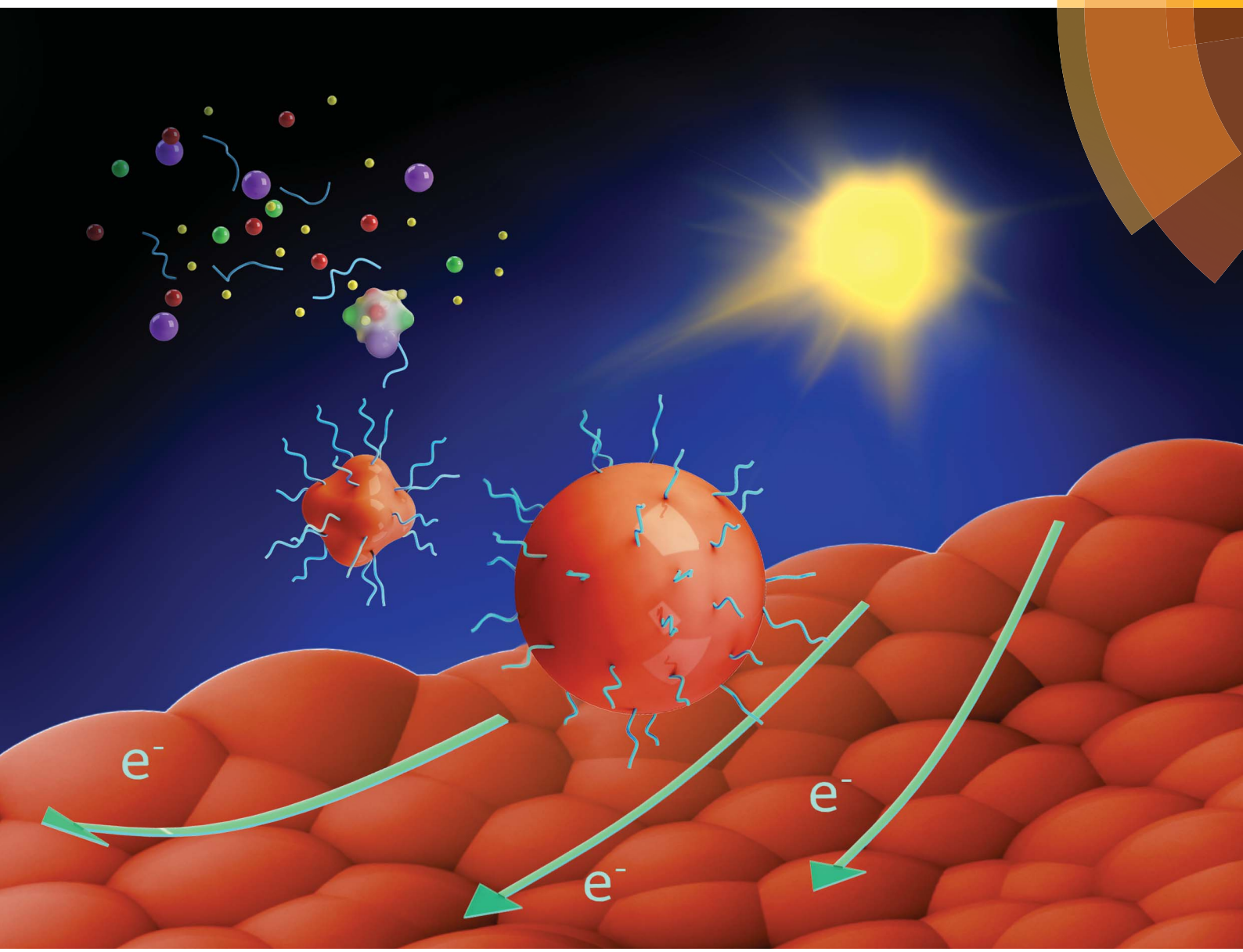

ISSN 2050-7488

ROYAL SOCIETY OF CHEMISTRY

PAPER

E. S. Aydil *et al.*

Rapid facile synthesis of Cu_2ZnSnS_4 nanocrystals

Journal of Materials Chemistry A

PAPER

View Article Online
View Journal | View Issue

Rapid facile synthesis of Cu_2ZnSnS_4 nanocrystals†

Cite this: *J. Mater. Chem. A*, 2014, **2**, 10389

B. D. Chernomordik, A. E. Béland, N. D. Trejo, A. A. Gunawan, D. D. Deng, K. A. Mkhoyan and E. S. Aydil*

Received 5th April 2014
Accepted 2nd May 2014

DOI: 10.1039/c4ta01658k

www.rsc.org/MaterialsA

Cu_2ZnSnS_4 (CZTS) nanocrystals were synthesized *via* thermolysis of single-source cation and sulfur precursors copper, zinc and tin diethyldithiocarbamates. The average nanocrystal size could be tuned between 2 nm and 40 nm, by varying the synthesis temperature between 150 °C and 340 °C. The synthesis is rapid and is completed in less than 10 minutes. Characterization by X-ray diffraction, Raman spectroscopy, transmission electron microscopy and energy dispersive X-ray spectroscopy confirm that the nanocrystals are nominally stoichiometric kesterite CZTS. The ~2 nm nanocrystals synthesized at 150 °C exhibit quantum confinement, with a band gap of 1.67 eV. Larger nanocrystals have the expected bulk CZTS band gap of 1.5 eV. Several micron thick films deposited by drop casting colloidal dispersions of ~40 nm CZTS nanocrystals were crack-free, while those cast using 5 nm nanocrystals had micron-scale cracks.

Introduction

Copper zinc tin sulfide (Cu_2ZnSnS_4 or CZTS) is an emerging material for thin film solar cells comprised of sustainable earth abundant elements.[1,2] A potentially low cost approach for making thin CZTS films relies on coating suitable substrates with a thin layer of CZTS nanocrystals from colloidal dispersions and then annealing this layer to form a polycrystalline film. Several CZTS nanocrystal synthesis methods have been reported, including solvothermal,[3,4] microwave-assisted,[5,6] and hot-injection.[7–9] Most methods require one hour (or longer) for synthesis and produce an average crystal size between ~5 and ~25 nm. CZTS nanocrystals smaller than ~3 nm in diameter exhibit quantum confinement, which introduces opportunities for band-gap tunable devices with sustainable and non-toxic materials.[10,11] On the other hand, a significant challenge for nanocrystal dispersion based thin film deposition techniques is cracking due to capillary stresses that develop during drying. These cracks are undesirable because they may lead to electrical shorts. Because the capillary forces are inversely proportional to the particle radius, increasing the particle size is one way to reduce the likelihood of crack formation. Herein, we report a rapid and facile CZTS nanocrystal synthesis using a hot-injection approach with thermally decomposable precursors wherein the average nanocrystal size can be controlled between ~2 nm and ~40 nm with one variable—temperature—and the total reaction and growth time is limited to less than 10 minutes.

Department of Chemical Engineering and Materials Science, University of Minnesota, Minneapolis, Minnesota 55455, USA. E-mail: aydil@umn.edu

† Electronic supplementary information (ESI) available: Additional characterization data, such as XRD and Raman, corresponding to SEMs *etc.* See DOI: 10.1039/c4ta01658k

Experimental

Materials

Oleic acid (technical grade, 90%), oleylamine (technical grade, 70%), 1-octadecene (technical grade, 90%), toluene (HPLC grade, 99.9%), sodium diethyldithiocarbamate trihydrate (ACS reagent, Sigma Aldrich), copper(II) chloride dihydrate (ACS grade, 99+%), zinc chloride (reagent grade, 98%), and tin(IV) chloride pentahydrate (98%) were purchased from Sigma-Aldrich. Reagent alcohol (histological grade, 90% ethyl alcohol, 5% methyl alcohol, 5% butyl alcohol) was purchased from Fisher Scientific. Quartz polished plates were purchased from GM Associates, Inc.

Colloidal CZTS nanocrystal synthesis

The cation and sulfur sources were copper(II) diethyldithiocarbamate, zinc(II) diethyldithiocarbamate, and tin(IV) diethyldithiocarbamate. Henceforth, these molecules are referred to as the precursors and labeled as $Cu(dedc)_2$, $Zn(dedc)_2$, and $Sn(dedc)_4$, respectively. Each of the three precursors were synthesized from their respective chloride salt (*i.e.*, copper(II) chloride, zinc chloride, or tin(IV) chloride) and sodium diethyldithiocarbamate. The details of the precursor synthesis are provided in the ESI.†

The precursor powder amounts were chosen based on the desired stoichiometry. Using 54 mg of $Cu(dedc)_2$, 27.2 mg $Zn(dedc)_2$, and 53.4 mg of $Sn(dedc)_4$ yields ~30 mg of stoichiometric Cu_2ZnSnS_4 nanocrystals. Typically, $Zn(dedc)_2$ powder is sticky and care must be taken to minimize its loss during transfer to the flask. We found that adjusting $Zn(dedc)_2$ mass to 28 mg gave near stoichiometric CZTS. The three precursor powders were mixed with 4 mL of oleic acid and 1 mL of 1-octadecene. One may instead use 5 mL of oleic acid without

1-octadecene to the same effect. It is important that the oleic acid is colorless or very faint yellow. Nanocrystals larger than ~15 nm (determined by X-ray diffraction) could not be synthesized at 280 °C when the oleic acid, as received from the supplier, was yellow. (Oleic acid may take on a yellow color when oxidized through air exposure during storage or purification.) While stirring vigorously, the precursor mixture was heated to 60 °C, degassed at 10 mTorr for several minutes, and purged with dry nitrogen gas to remove the air from the flask. The degassing and purge steps were repeated thrice. After the last purge, the precursor mixture was heated to 140 °C under continuous flow of dry nitrogen gas. As the temperature rises, the solid precursor powders dissolve, with $Sn(dedc)_4$ being the last one to do so. All of the solids are completely dissolved within one minute of reaching 140 °C. It is important not to let the precursor solution reach 175 °C to avoid formation of binary tin sulfide precipitates (*i.e.* SnS_2) due to the premature decomposition of $Sn(dedc)_4$. The precursor solution was then cooled and held at 75 °C. Separately, 10 mL of oleylamine was also similarly degassed and purged thrice at 60 °C before heating it to the desired synthesis temperature between 150–340 °C, while stirring. The synthesis temperature determines the average nanocrystal size. The precursor mixture (itself at 75 °C) was then extracted *via* syringe and swiftly injected into the flask containing the hot oleylamine. The reaction solution immediately turned black and then vigorously bubbled and fumed for several minutes. Upon injection, the reaction solution temperature dropped by 10–15% but rose to the original oleylamine temperature within two minutes. After injection, the solution was kept on the heater for a total of ten minutes. However, growth times of several minutes to one hour produced the same result. The reaction solution was then cooled to room temperature by immersing the flask in a cold water bath. Although keeping the precursor solution at 140 °C (instead of 75 °C) would decrease the temperature drop the solution experiences upon injection, the precursor solution was cooled to 75 °C to limit the handling of hot organics during injection.

The CZTS nanocrystals were precipitated by adding ~30 mL of reagent alcohol and centrifuging for five minutes. After discarding the supernatant, the CZTS nanocrystals were dispersed in ~1 mL toluene by sonication for several minutes after adding ~0.3 mL of neat oleic acid. The nanocrystals were then washed a second time by adding ~20 mL reagent alcohol and centrifuging for five minutes. Following, the colorless supernatant was discarded and the CZTS nanocrystals were redispersed in 1 mL toluene with 0.01 vol% oleic acid and sonicated for one hour. The reasons for adding oleic acid (0.3 mL) before the second washing step and for using toluene with 0.01 vol% oleic acid are discussed in the ESI.†

Film preparation and annealing

CZTS nanocrystal dispersions (30 mg mL^{-1}) were drop cast into a volume formed by a 250 μm thick stainless steel frame clasped onto a 1 in. × 1 in. substrate (*e.g.*, quartz or molybdenum-coated soda lime glass) using binder clips. A plastic funnel, with a micropipette tip attached to its narrow end, was inverted over the film. The frame pins the drying front at the edges of the frame and the funnel slows the drying; this approach eliminated the formation of drying patterns such as "coffee rings."[12] The film was dried in a fume hood for one hour. After drying, the NC film was 2–3 μm thick. Digital photograph(s) of film preparation are included in the ESI Fig. S2.†

Solar cell preparation

CZTS nanocrystals synthesized with Cu/(Zn + Sn) and Zn/Sn ratios of 0.89 and 1.08, respectively, were drop cast onto soda lime glass (SLG) substrates coated with 400 nm thick sputtered molybdenum film. The CZTS nanocrystal films on Mo-coated SLG and 14 mg of solid sulfur were sealed in evacuated quartz ampoules. The ampoules were annealed in a furnace pre-heated to 600 °C. The oven was turned off after 1 hour and allowed to cool naturally before removing the ampoules.[13] The solar cells were completed by depositing ≈185 nm thick CdS, ≈100 nm thick i-ZnO and 250 nm thick indium tin oxide sequentially on the annealed CZTS film by chemical bath deposition,[14] RF sputtering, and DC sputtering, respectively. The top contacts were formed by DC sputtering 50 nm of Ni followed by 1 μm of Al. Details of the deposition conditions are given in the ESI.†

Characterization

X-ray diffraction (XRD) from the nanocrystal film was collected using a Bruker D8 Discover equipped with a 2D Hi-Star area detector. The X-ray beam was collimated to an 800 μm spot. Raman spectra were collected using a WiTec alpha300R confocal Raman microscope equipped with a UHTS300 spectrometer and a DV401 CCD detector. An Omnichrome argon ion laser (514.5 nm) was used to illuminate the sample and the beam size was ~300 nm. Raman scattering was collected in a backscattering geometry using an 1800 lines per mm grating. The spectra resolution was ~1.3 cm^{-1}. For all measurements the laser intensity was turned low enough to prevent spectral distortion or peak shifting as a result of local heating. The elemental composition of the CZTS nanocrystals and the atomic carbon concentration were measured using a Thermo-Noran Vantage energy dispersive X-ray spectrometer (EDS) installed within a JEOL 6500 field-emission scanning electron microscope (SEM). The electron energy was 15 keV for all EDS measurements. Transmission electron microscope (TEM) images were recorded using an FEI Tecnai G2 F30 S-TEM system with a Schottky field-emission electron gun operated at 200 kV accelerating voltage.[15] The solar cells were illuminated with simulated sunlight at 100 mW cm^{-2} using a Xe-arc lamp and AM 1.5 filters from Newport.[16] More details about characterization are provided in the ESI.† The illuminated area, excluding contacts, was 0.22 cm^2. The current–voltage (*J*–*V*) characteristics were measured using a Keithley 2400 SourceMeter.

Results and discussion

When heated separately in a neat solvent, $Cu(dedc)_2$, $Zn(dedc)_2$, and $Sn(dedc)_4$ decompose into their respective binary metal

sulfides, Cu_2S, ZnS, and SnS_2, and the decomposition begins at different temperatures for each molecule: $Zn(dedc)_2$, at 240 °C, $Cu(dedc)_2$ at 220 °C, and $Sn(dedc)_4$ at 175 °C.[10] In the presence of oleylamine, however, the temperature at which metal alkyldithiocarbamate molecules decompose is reduced to less than 150 °C.[10,17,18] Jung *et al.*[17] proposed that oleylamine accelerates the decomposition of metal alkyldithiocarbamate complexes through coordination with the thiocarbonyl carbon of the dithiocarbamate ligand. Oleic acid, on the other hand, acts as a surface-stabilizing ligand for the nuclei. The ratio of the two molecules—the nuclei-forming oleylamine and the surface-stabilizing oleic acid—can be manipulated to affect the final particle size and shape.[17,19,20] When oleylamine and the three metal diethyldithiocarbamates are mixed in a solvent, CZTS nucleates if the local temperature is above the decomposition temperature of all three precursor molecules in presence of oleylamine (~150 °C).

In previously published adaptations of this synthesis approach, oleylamine was injected into a heated mixture of metal alkyldithiocarbamate molecules.[10,18] This approach was used to synthesize 2–7 nm CZTS nanocrystals by varying both the reaction temperature and the volume of oleylamine injected into the heated precursors.[10] Largest nanocrystals (7 nm) were obtained by increasing the reaction temperature (between 150 °C and 175 °C) and/or decreasing the volume of injected oleylamine (4 mL for 2 nm nanocrystals and 0.5 mL for 5 nm nanocrystals). In this approach, the maximum nanocrystal size is limited to less than 7 nm by the decomposition temperature of $Sn(dedc)_4$ (175 °C in absence of oleylamine): if the mixture of metal alkyldithiocarbamate solution is heated above this temperature, SnS_2 nanocrystals are obtained in addition to CZTS. One way to eliminate this restriction is to use tin alkyldithiocarbamates with different alkyl groups.[21] For example, tin(IV) dibutyldithiocarbamate decomposes at ~280 °C.[22] However, the use of other alkyldithiocarbamate molecules increases the complexity and toxicity of the chemistry. For example, synthesis of tin(IV) dibutyldithiocarbamate requires the use of toxic dibutyltin dichloride.

Instead of the above approaches, a wider range of reaction temperatures, and therefore larger variation in CZTS nanocrystal sizes, is achieved by injecting the metal diethyldithiocarbamate solution into hot oleylamine. Upon injection, all three metal diethyldithiocarbamate complexes decompose simultaneously and form CZTS nanocrystals. The average CZTS nanocrystal size can be varied from ~2 to 40 nm by adjusting the oleylamine temperature between 150 and 340 °C, without needing to change other variables such as oleylamine volume, nanocrystal composition, or growth time.

Fig. 1 shows the XRD from CZTS nanocrystals synthesized at 150 °C, 210 °C, 280 °C, and 340 °C (the temperature, T, of the solution at the time of injection). The diffraction peak widths decrease with increasing synthesis temperature because the synthesis yields larger crystals at higher temperatures. All XRD patterns match the expected diffraction pattern for kesterite CZTS (ICDD-ref 04-005-0388, also shown in Fig. 1) though the width of the diffraction peaks broaden with decreasing size and several diffraction peaks begin to overlap. The diffraction peaks

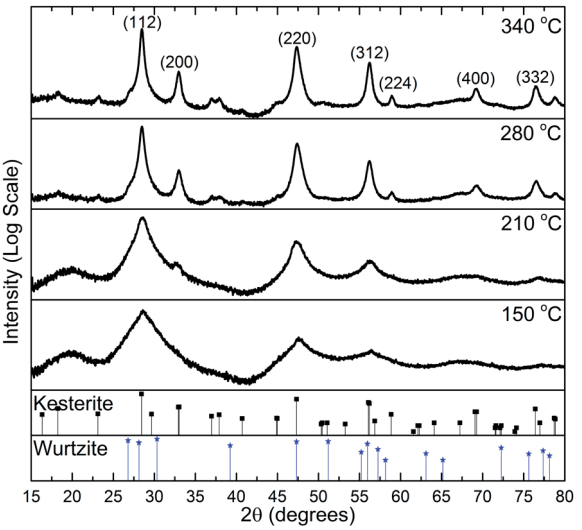

Fig. 1 XRD from CZTS nanocrystals synthesized at 150 °C, 210 °C, 280 °C, and 340 °C. The XRD patterns match that of kesterite CZTS. A minority of nanocrystals may have the wurtzite structure.

at 37.0° [(202)], 37.9° [(211)], and 44.9° [(105) and (213)] are clearly resolved in the largest nanocrystals and indicate the unambiguous presence of CZTS. These peaks are absent and very weak in ZnS and tetragonal Cu_2SnS_3, respectively, which otherwise have similar diffraction patterns to CZTS.[23,24] The broad peak at ~20°, which only appears for nanoparticles synthesized at $T \leq 210$ °C, is due to oleylamine and oleic acid capping ligands.[10,25] The volume fraction of the ligands is higher for small nanocrystals and diffraction from oleylamine and oleic acid become detectable. A weak shoulder at 26.9° becomes discernible in the XRD patterns from nanocrystals synthesized at $T \geq 280$ °C. The location of this shoulder matches the wurtzite CZTS (100) diffraction peak. (The wurtzite CZTS XRD pattern was calculated based on the wurtzite ZnS (2H) crystal structure—space group $P6_3mc$—by replacing the Zn(II) with Cu(I), Zn(II), and Sn(IV).)[26] This may indicate that a minority of CZTS nanocrystals has the wurtzite crystal structure. Other wurtzite CZTS peaks overlap with kesterite CZTS diffractions. Indeed, the wurtzite CZTS phase has been observed in other CZTS nanocrystal synthesis approaches.[26–29] The wurtzite shoulder disappears after films cast from dispersions of these nanocrystals are annealed at temperatures high enough for grain growth (*e.g.*, 600 °C as shown in ESI Fig. S3†). This is consistent with this peak arising from the thermodynamically less stable wurtzite CZTS phase.[30]

The presence of any significant amounts of ZnS, including wurtzite ZnS, and tetragonal Cu_2SnS_3 are ruled out using Raman spectroscopy. Fig. 2 compares the Raman spectra from nanocrystals synthesized at 150 °C, 210 °C, 280 °C, and 340 °C. The nanocrystals synthesized at $T \leq 210$ °C exhibit a single Raman scattering peak centered at 337 cm^{-1}, the expected value for CZTS. The linewidths are broad due to phonon confinement in small nanocrystals, which has also been observed for other materials.[31] The larger nanocrystals grown at $T \geq 280$ °C exhibit narrower Raman scattering linewidths: the A_1 modes at

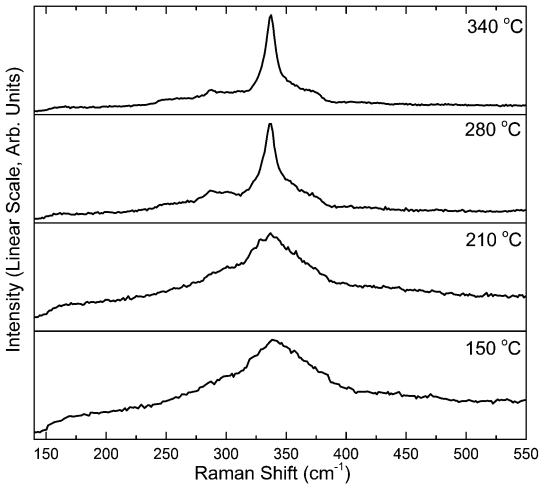

Fig. 2 Raman spectra from nanocrystals synthesized at 150 °C, 210 °C, 280 °C, and 340 °C. The peak widths vary due to the differences in nanocrystal sizes. The strongest peak in each of the spectra is centered at 337 cm^{-1}, the expected CZTS Raman scattering wavenumber.

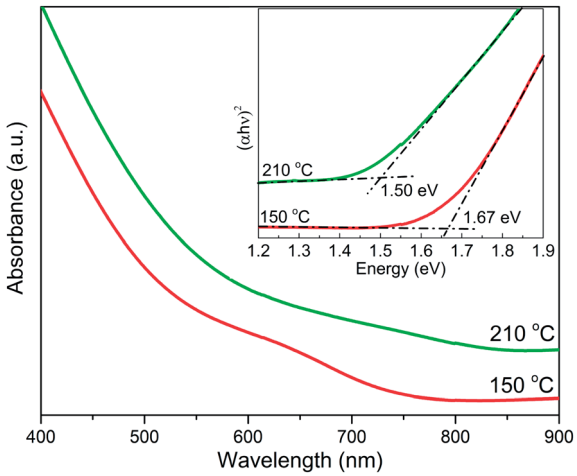

Fig. 3 Room temperature optical absorption spectra for CZTS nanocrystal dispersions synthesized at 150 °C and 210 °C. The inset shows the Tauc plot for the corresponding absorbance curves. The absorption edge of nanocrystals synthesized at 150 °C is blue-shifted due to quantum confinement. The spectra have been offset in *y*-axis for clarity. The long wavelength asymptotes correspond to the zero absorption baseline.

337 cm^{-1} and 287 cm^{-1} are better defined and the characteristic shoulder at 345–380 cm^{-1} (B and E modes) emerges.[24] Raman scattering corresponding to Cu_2S (475 cm^{-1}) is not present. Raman scattering from ZnS (350 cm^{-1}), and SnS_2 (315 cm^{-1}), if present, is much less than that from CZTS. Even single crystal CZTS exhibits a weak shoulder at 350 cm^{-1} and weak featureless Raman scattering between 287 cm^{-1} and 337 cm^{-1},[32] which overlaps with the expected Raman peaks of ZnS and SnS_2. The absence of SnS_2 XRD peaks indicates that SnS_2 volume fraction is below the detection limit of XRD. However, it is difficult to conclusively rule out small amounts of ZnS.

EDS was used to analyze the elemental stoichiometry of the nanocrystals. The precursor concentrations given in the Experimental section produced nanocrystals with 2 : 1 : 1 : 4 elemental ratios of Cu : Zn : Sn : S. The stoichiometry may be easily tuned (*e.g.*, slightly Cu poor or Zn rich) around stoichiometric CZTS by varying the molar ratios of precursor powders used in the synthesis. We thus conclude that the nanocrystals are nominally phase-pure CZTS, at least within the detection limits of XRD and Raman scattering.

The sizes of the nanocrystals synthesized at 150 °C, 210 °C, 280 °C and 340 °C were 2 nm, 5 nm, 24 nm, and 40 nm, respectively, as calculated from the widths of the (112) diffraction peaks (at 28.48°) using Scherrer analysis. The absorption spectrum of the nanocrystals synthesized at 150 °C suggests a CZTS nanocrystal size between 2 and 2.5 nm, consistent with the Scherrer analysis. As shown in Fig. 3, the latter nanocrystals exhibit an absorption edge that is shifted to higher energies relative to that of larger nanocrystals, a shift characteristic of quantum confinement. From the Tauc plot in the Fig. 3 inset, the band gap of the nanocrystals synthesized at 150 °C is estimated to be 1.67 eV. This is consistent with measurements by Khare *et al.*[10] who reported effective band gaps of 1.63 eV and 1.8 eV for 2.5 nm and 2 nm diameter nanocrystals, respectively. Thus, the average size of the nanocrystals synthesized at 150 °C is between 2 and 2.5 nm. The nanocrystals synthesized at higher temperatures are larger than the Bohr radius of CZTS (~3 nm)[3,10] and therefore have the same band gap as bulk CZTS (1.5 eV). The absorption spectrum of the nanocrystals synthesized at 210 °C is shown in Fig. 3 as an example. The larger nanocrystals synthesized at $T \geq 240$ °C agglomerate and are difficult to disperse: they appear turbid and produce absorption spectra convoluted by scattering.

TEM images of nanocrystals synthesized at 280 °C are shown in Fig. 4. The lattice spacing in the nanocrystals in Fig. 4a and b is 3.14 ± 0.01 Å, which corresponds to the (112) plane spacing of kesterite CZTS. The lattice spacing in the inset of Fig. 4b is 1.92 ± 0.01 Å, which corresponds to the (204) and (220) plane spacings. The larger nanocrystals (>15 nm, *e.g.*, Fig. 4a) tend to be faceted and non-spherical while the smaller nanocrystals (<10 nm, *e.g.*, Fig. 4b) tend to be spherical. For example, the nanocrystal in Fig. 4a is 26 nm along the [112] direction, nearly the same as the crystallite size (24 nm) calculated from the width of the (112) XRD peak. Indeed, for nanocrystals synthesized at $T \geq 280$ °C, the (112) XRD peak yields the largest crystallite sizes while other XRD peaks yield smaller sizes [*e.g.*, 14 nm from (204) and (220) planes, 15 nm from the (200) plane, and 19 nm from (312) and (116) planes for nanocrystals synthesized at 280 °C]. This variation of the crystallite size calculated from different crystal planes is consistent with the dimensions and nonspherical shapes observed with TEM: the nanocrystals are larger along [112] direction than other directions. TEM images also indicate a broad distribution of nanocrystal sizes, from 5 nm to 30 nm. (Additional TEM images are shown in ESI Fig. S4†.) The nanocrystals synthesized at 340 °C are large enough to be observed using SEM (Fig. 4c). Similarly, there is a broad distribution of nanocrystal sizes, ranging from 10 nm to 100 nm. The average nanocrystal size in Fig. 4c,

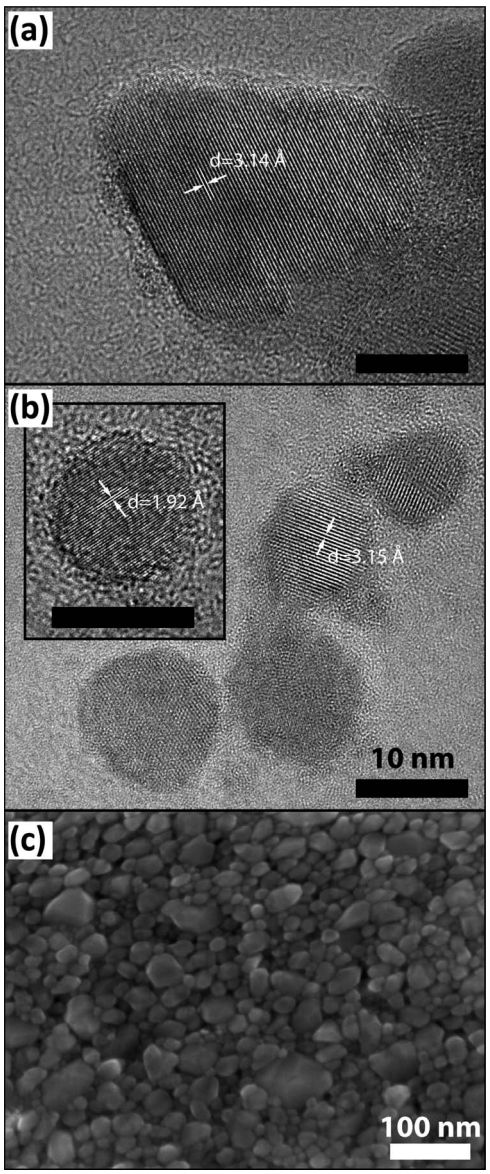

Fig. 4 High resolution TEM images of CZTS nanocrystals synthesized at 280 °C. The nanocrystals are single-crystalline. Black scale bars in (a) and (b) are 10 nm. (c) SEM image of a film of CZTS nanocrystals synthesized at 340 °C: the average crystal size is 42 nm.

measured by averaging the number of grains along randomly chosen lines, is 42 nm, in close agreement with the crystallite size determined from the Scherrer analysis of the XRD peaks (40 nm).

Fig. 5 shows the average nanocrystal size as a function of the synthesis temperature. The nanocrystal size increases gradually between 150 and 210 °C but faster between 210 and 280 °C. One possible explanation for the faster growth between 210 and 280 °C is that oleic acid and oleylamine react at ~250 °C to form oleyloleamide[19] and the presence of oleyloleamide has been shown to increase the nanocrystal size in systems where the cations are coordinated with acetylacetonate.[20]

One application of these nanocrystals is in the synthesis of polycrystalline thin films for solar cells. Layers formed by a

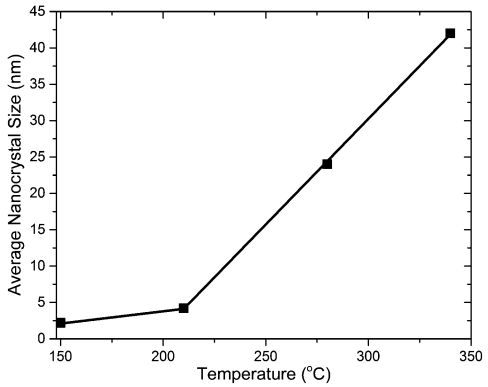

Fig. 5 Average nanocrystal size as a function of synthesis temperature.

suitable coating method (*e.g.*, drop casting, spin coating, *etc.*) are annealed to form polycrystalline films with micron size grains. Cracking in nanocrystal coatings is a problem for most applications, especially for solar cells. Cracks can lead to electrical shorts between device layers and high shunt currents. Crack formation during drying of a nanocrystal film cast from a dispersion is complex and depends on many variables, such as the nanocrystal size, film thickness, solvent evaporation rate, size and coverage of ligand molecules, and the substrate.[33–37] For example, Fig. 6a shows a film drop cast from a dispersion of 5 nm CZTS nanocrystals on a molybdenum-coated quartz substrate. After drying, micron wide cracks appear and the 2 μm thick film breaks up into ~10 μm × ~15 μm islands. The films crack because capillary pressure between the particles leads to stresses within the film during drying.[34] Cracking can be eliminated by increasing the concentration of oleic acid in the colloidal dispersion (see Fig. S5a and S5b in ESI;† other film deposition methods are also discussed in ESI Fig. S6–S8†). The oleic acid reduces cracking by acting as a compliant medium between the particles: oleic acid coronas around the nanocrystals deform and relax the stresses that may otherwise build up within the film.[38] For thin film solar cells, the nanocrystal coatings need to be annealed to promote grain growth. During annealing, a significant fraction of the ligand molecules desorb and/or thermally decomposes into volatile species.[13] (Carbon concentration in films is measured by EDS and is found to be reduced.) The removal of the organic ligands, in addition to concurrent coarsening of the nanocrystals, results in the film experiencing significant volume loss. The film shrinkage contributes to stresses that induce cracking during the annealing process (see ESI Fig. S5c†).

Increasing the nanocrystal size prevents film cracking during drying and annealing. Crack formation is inhibited during drying because the capillary pressure is inversely proportional to nanocrystal radius. For example, Fig. 6b and c show plan view and cross-sectional SEM images of a ~2 μm thick nanocrystal film drop cast from a dispersion of ~42 nm nanocrystals (synthesized at 340 °C). The film cast from these large nanocrystals is completely crack-free. Increasing nanocrystal size also reduces the volume loss associated with evaporation and

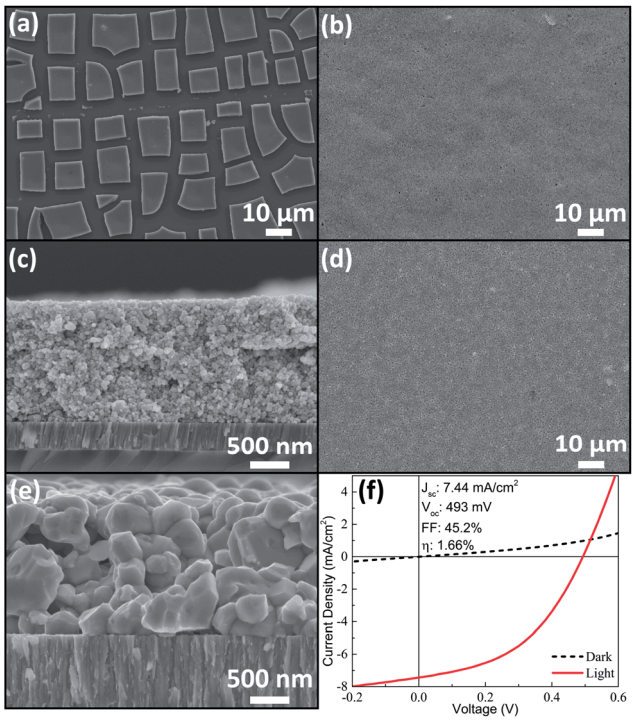

Fig. 6 SEM images of CZTS nanocrystal films drop cast onto molybdenum-coated quartz substrates using 30 mg mL^{-1} dispersions of (a) 5 nm nanocrystals and (b) ~42 nm nanocrystals. (c) Cross-section SEM image of ~42 nm nanocrystals on molybdenum coated SLG. (d) Plan view and (e) cross-sectional SEM images after annealing a film consisting of ~42 nm nanocrystals. (f) *J–V* characteristics of solar cell made from the film shown in (d) & (e) under dark (dashed) and AM1.5 light (solid) conditions.

decomposition of the organic ligands during annealing. For example, assuming close packed nanocrystals with 1 nm ligand shells, the solid volume increases from 27% to 64% when the nanocrystals size is increased from 5 nm to 40 nm (ESI Fig. S9†). Indeed, Fig. 6d shows that a film cast from ~42 nm nanocrystals remains crack-free even after annealing (1 hour at 600 °C on molybdenum-coated SLG), during which the nanocrystals coarsen and sinter (Fig. 6e). Moreover, the broad distribution of nanocrystal sizes may impart further advantages toward reduction in cracks: film shrinkage due to coarsening and densification during annealing is reduced when smaller nanocrystals fill the interstitial voids between the large nanocrystals.

Fig. 6f shows *J–V* characteristics of a 1.66% efficient solar cell made with the annealed crack-free film shown in Fig. 6d and e (see also ESI Fig. S10†). The characteristics represent an unoptimized solar cell: for example, performance may be improved further by reducing the thicknesses of the CdS layer, optimizing the Cu/(Zn + Sn) and Zn/Sn ratios, and shortening the annealing time to reduce the MoS_2 thickness.

Conclusions

In summary, we describe a method for rapid (≤10 min) synthesis of 2–40 nm diameter CZTS nanocrystals by varying only the synthesis temperature between 150 °C and 340 °C. The 2 nm nanocrystals synthesized at 150 °C exhibit quantum confinement with an effective band gap of 1.67 eV. Nanocrystals synthesized at higher temperatures have a band gap of 1.5 eV. Films cast from dispersions of small (*e.g.*, 5 nm) nanocrystals exhibit cracks but these cracks are eliminated when dispersions of larger nanocrystals (*e.g.*, 40 nm) are used. The films with larger nanocrystals, which remained crack-free after annealing, were used to make a thin film solar cell.

Acknowledgements

This work was supported primarily by the MRSEC Program of the US National Science Foundation (NSF) under Award Number DMR-0819885 and partially by the Initiative for Renewable Energy & the Environment, IREE (RL-0004-11). B.D.C. acknowledges financial support from the NSF Graduate Research Fellowship Program. Parts of this work were completed at the Characterization Facility at the University of Minnesota, which receives partial support from NSF through the MRSEC program.

Notes and references

1 C. A. Wolden, J. Kurtin, J. B. Baxter, I. Repins, S. E. Shaheen, J. T. Torvik, A. A. Rockett, V. M. Fthenakis and E. S. Aydil, *J. Vac. Sci. Technol., A*, 2011, **29**, 030801.
2 S. Abermann, *Sol. Energy*, 2013, **94**, 37–70.
3 W. C. Liu, B. L. Guo, X. S. Wu, F. M. Zhang, C. L. Mak and K. H. Wong, *J. Mater. Chem. A*, 2013, **1**, 3182–3186.
4 M. Cao and Y. Shen, *J. Cryst. Growth*, 2011, **318**, 1117–1120.
5 B. Flynn, W. Wang, C. Chang and G. S. Herman, *Phys. Status Solidi A*, 2012, **209**, 2186–2194.
6 S. W. Shin, J. H. Han, Y. C. Park, G. L. Agawane, C. H. Jeong, J. H. Yun, a. V. Moholkar, J. Y. Lee and J. H. Kim, *J. Mater. Chem.*, 2012, **22**, 21727–21732.
7 Q. Guo, H. W. Hillhouse and R. Agrawal, *J. Am. Chem. Soc.*, 2009, **131**, 11672–11673.
8 K.-L. Ou, J.-C. Fan, J.-K. Chen, C.-C. Huang, L.-Y. Chen, J.-H. Ho and J.-Y. Chang, *J. Mater. Chem.*, 2012, **22**, 14667–14673.
9 C. Zou, L. Zhang, D. Lin, Y. Yang, Q. Li, X. Xu, X. Chen and S. Huang, *CrystEngComm*, 2011, **13**, 3310–3313.
10 A. Khare, A. W. Wills, L. M. Ammerman, D. J. Norris and E. S. Aydil, *Chem. Commun.*, 2011, **47**, 11721–11723.
11 T. J. Pundsack, B. D. Chernomordik, A. E. Béland, E. S. Aydil and D. A. Blank, *J. Phys. Chem. Lett.*, 2013, **4**, 2711–2714.
12 R. D. Deegan, O. Bakajin, T. F. Dupont, G. Huber, S. R. Nagel and T. A. Witten, *Nature*, 1997, **389**, 827–829.
13 B. D. Chernomordik, A. E. Béland, D. D. Deng, L. F. Francis and E. S. Aydil, *Chem. Mater.*, DOI: 10.1021/cm500791a.
14 B. S. Tosun, C. Pettit, S. A. Campbell and E. S. Aydil, *ACS Appl. Mater. Interfaces*, 2012, **4**, 3676–3684.
15 M. J. Behr, K. A. Mkhoyan and E. S. Aydil, *ACS Nano*, 2010, **4**, 5087–5094.
16 K. S. Leschkies, R. Divakar, J. Basu, E. Enache-Pommer, J. E. Boercker, C. B. Carter, U. R. Kortshagen, D. J. Norris and E. S. Aydil, *Nano Lett.*, 2007, **7**, 1793–1798.

17 Y. K. Jung, J. Il Kim and J.-K. Lee, *J. Am. Chem. Soc.*, 2010, **132**, 178–184.
18 D. Pan, L. An, Z. Sun, W. Hou, Y. Yang, Z. Yang and Y. Lu, *J. Am. Chem. Soc.*, 2008, **130**, 5620–5621.
19 W. Niu, S. Wu and S. Zhang, *J. Mater. Chem.*, 2011, **21**, 10894–10902.
20 H. Wu, Y. Yang and Y. C. Cao, *J. Am. Chem. Soc.*, 2006, **128**, 16522–16523.
21 M. A. Malik, M. Afzaal and P. O'Brien, *Chem. Rev.*, 2010, **110**, 4417–4446.
22 K. Ramasamy, M. a. Malik and P. O'Brien, *Chem. Sci.*, 2011, **2**, 1170–1172.
23 A.-J. Cheng, M. Manno, A. Khare, C. Leighton, S. A. Campbell and E. S. Aydil, *J. Vac. Sci. Technol., A*, 2011, **29**, 051203.
24 A. Khare, B. Himmetoglu, M. Johnson, D. J. Norris, M. Cococcioni and E. S. Aydil, *J. Appl. Phys.*, 2012, **111**, 083707.
25 A. Pein, M. Baghbanzadeh, T. Rath, W. Haas, E. Maier, H. Amenitsch, F. Hofer, C. O. Kappe and G. Trimmel, *Inorg. Chem.*, 2011, **50**, 193–200.
26 X. Lu, Z. Zhuang, Q. Peng and Y. Li, *Chem. Commun.*, 2011, **47**, 3141–3143.
27 A. Singh, H. Geaney, F. Laffir and K. M. Ryan, *J. Am. Chem. Soc.*, 2012, **134**, 2910–2913.
28 M. D. Regulacio, C. Ye, S. H. Lim, M. Bosman, E. Ye, S. Chen, Q.-H. Xu and M.-Y. Han, *Chemistry*, 2012, **18**, 3127–3131.
29 M. Li, W.-H. Zhou, J. Guo, Y.-L. Zhou, Z.-L. Hou, J. Jiao, Z.-J. Zhou, Z.-L. Du and S.-X. Wu, *J. Phys. Chem. C*, 2012, **116**, 26507–26516.
30 S. Chen, A. Walsh, Y. Luo, J.-H. Yang, X. G. Gong and S.-H. Wei, *Phys. Rev. B: Condens. Matter Mater. Phys.*, 2010, **82**, 195203.
31 D. Bersani, P. P. Lottici and X.-Z. Ding, *Appl. Phys. Lett.*, 1998, **72**, 73–75.
32 D. Dumcenco and Y. Huang, *Opt. Mater.*, 2013, **35**, 419–425.
33 A. F. Routh, *Rep. Prog. Phys.*, 2013, **76**, 046603.
34 W. P. Lee and A. F. Routh, *Langmuir*, 2004, **20**, 9885–9888.
35 M. S. Tirumkudulu and W. B. Russel, *Langmuir*, 2004, **20**, 2947–2961.
36 K. Singh and M. Tirumkudulu, *Phys. Rev. Lett.*, 2007, **98**, 218302.
37 M. S. Tirumkudulu and W. B. Russel, *Langmuir*, 2005, **21**, 4938–4948.
38 T. Kanai and T. Sawada, *Langmuir*, 2009, **25**, 13315–13317.